Indian J Phys
https://doi.org/10.1007/s12648-025-03663-4

ORIGINAL PAPER

The investigation of structural, elastic, electronic, vibrational, thermo-physical, and optical properties of hexagonal-type X_2N (X = Mn, Tc, and Re) compounds

C Kürkçü[1]* and Ç Yamçıçıer[2]

[1]Department of Electronics and Automation, Kırşehir Ahi Evran University, Kırşehir, Turkey

[2]Department of Electricity and Energy, Osmaniye Korkut Ata University, Osmaniye, Turkey

Received: 09 July 2024 / Accepted: 16 May 2025

Abstract: The structural, elastic, electronic, phonon, thermo-physical, and optical properties of hexagonal-type X_2N (X = Mn, Tc, and Re) compounds were studied within the framework of density functional theory using the generalized gradient approximation (GGA). The obtained lattice parameter values were in good agreement with the literature. To investigate the mechanical stability of the studied compounds, the elastic constant values of the three compounds were calculated and from these values, some stiffness constant values such as Bulk (317.49 GPa, 339.29 GPa, and 401.57 GPa for Mn_2N, Tc_2N, and Re_2N, respectively), Young's (443.14 GPa, 438.11 GPa, and 542.84 GPa for Mn_2N, Tc_2N, and Re_2N, respectively), Shear modulus (174.83 GPa, 170.50 GPa, and 212.93 GPa for Mn_2N, Tc_2N, and Re_2N, respectively) values, and Poisson's ratio (0.27, 0.28, and 0.27 for Mn_2N, Tc_2N, and Re_2N, respectively), were also obtained. According to the calculated elastic constant values, all compounds are mechanically stable and ductile. In addition, the atoms are interconnected by ionic bonding. Electronic band structure calculation was performed to reveal the types of materials. All compounds were found to have metallic character due to the absence of a band gap. Phonon calculation was also performed, which gives information about the dynamic stability of the materials. X_2N (X = Mn, Tc, and Re) compounds were found to be dynamically stable since they have no negative branches. Thermophysical analyses revealed that Mn_2N has the highest Debye temperature of 760 K, thus indicating strong chemical bonding and high thermal conductivity. Finally, in optical investigations, the reflectivity, absorption, and optical conductivity properties of X_2N compounds were evaluated in detail, and it was found that these compounds have high absorption properties in the ultraviolet region.

Keywords: Electronic properties; Elastic properties; Phonon; Thermodynamic; Optical properties

Introduction

Metal nitrides (MNs) play a crucial role in semiconductors and are commonly used in electrocatalytic water-splitting, improved electrochemical energy storage, and surface-coating technologies[1–3]. MNs are a diverse set of materials, encompassing group-IIA nitrides, group-IIIA nitrides, and transition metal nitrides (TMNs), due to the different metal species and stoichiometry variations between nitrogen-lean and nitrogen-rich phases [4–6].

TMNs demonstrate exceptional physical characteristics compared to MNs, including high hardness and a high melting point, making them suitable for applications including cutting tools and protective coatings [7]. The Transition Metal Nitrides (TMNs) show potential as advanced electrochemical energy storage materials for lithium-ion batteries, sodium-ion batteries, and electrochemical supercapacitors. Furthermore, the exceptional physical and chemical features of TMNs make them appealing for applications in electrochemical catalysis, including the hydrogen evolution process, oxygen reduction reaction, and nitrogen reduction reaction [8–10].

Computational methods have projected a range of stable 2D transition metal nitride materials in recent years, establishing them as promising candidates [11–13]. When bulk structures of transition metal nitrides are reduced to ultrathin layers, they often exhibit planar structures to ensure structural stability, as a result of alterations in the coordination number of the bonded atoms [14]. In addition

*Corresponding author, E-mail: ckurkcu@ahievran.edu.tr

Published online: 13 June 2025

to the 2D TMNs, the group-IIIA nitrides and group-IIA nitrides also have their two-dimensional versions. 2D IIIANs with planar honeycomb structures, such as 2D AlN, GaN, and InN, are well-established 2D materials with different fabrication methods and real-world uses [15, 16]. Compared to other studies, research on 2D group-IIA nitrides is limited and primarily focused on theoretical aspects because of their reduced structural stability.

Computational techniques have projected a range of stable 2D TMNs materials in recent years, establishing them as promising candidates in the field. When the bulk structures of transition metal nitrides (TMNs) are reduced to ultrathin layers, they often adopt planar patterns to ensure structural stability. This is because the coordination number of the bonding atoms varies in these circumstances. In addition to the 2D TMNs, there are also two-dimensional counterparts of group-IIIA nitrides and group-IIA nitrides. The 2D group-IIIA nitrides, including 2D AlN, GaN, and InN, possess planar honeycomb structures and have been extensively studied due to their well-established synthetic methods and wide range of practical uses. In contrast, research on 2D group-IIA nitrides is limited and primarily focused on theoretical studies, primarily because of their comparatively reduced structural stability.

The current investigations have revealed significant potential applications of 2D MNs in several disciplines such as electronics, spintronics, sensing, catalysis, and energy storage. For example, the electronic band of certain two-dimensional metal nitrides (MNs) can be modified not only by changing the number of layers but also by applying an electric field or strain. This property makes them very suitable for use in semiconductor devices. A significant number of two-dimensional magnetic nanomaterials display inherent ferromagnetic properties, making them extremely attractive for the advancement of spintronic nanodevices in the future. Theoretical studies have shown that monolayers of group-IIIA nitrides have the potential to be used as sensing materials for detecting hazardous gas formaldehyde. Moreover, certain two-dimensional metal nitrides (2D MNs) exhibit potential as materials for light-emitting diodes (LEDs) and high-performance solar cells [17, 18].

The vibrational characteristics of hexagonal Re_2N were examined by Friedrich et al. [19] and Deligoz et al. [20]. Zhang et al. [21] subsequently conducted a study on the thermodynamic stability, mechanical characteristics, and bond deformation mechanism of Re_2N. Re_2N has been examined for its structural, electronic, and elastic characteristics under normal conditions [22–25]. It has been determined that Re_2N is an extremely resistant and rigid substance due to its elevated bulk modulus, which is a result of the robust covalent bonds between Re and N. The stability, electrical, and elastic properties of trigonal-type M_2N compounds (where M represents Cr, V, Nb, and Ta) are examined using first-principles calculations by Yu et al. [26].

As a result of the literature study, it was seen that some studies, such as structural, elastic, and electronic studies, have been carried out on the Re_2N compound. However, there are almost no studies on Tc_2N and Mn_2N. In addition, important physical properties of these three compounds, especially phonon, thermo-physical, and optical properties, have been calculated for the first time in this study. In this way, readers will be able to access information about these compounds in a single study without spending much time and will be able to use the results in their experimental and theoretical studies.

The aim of this study is to comprehensively investigate the physical properties of hexagonal X_2N (X = Mn, Tc, and Re) compounds and reveal their scientific and technological potential. First, the structural parameters of the compounds in their lowest energy states were calculated and compared with the results reported in the literature, ensuring the accurate modeling of their structural characteristics.

The mechanical properties, such as mechanical stability and ductility or brittleness, were examined through elastic constants, and the bonding nature between the atoms was determined. The electronic band structure was analyzed to evaluate whether the compounds exhibit metallic or semiconducting characteristics, shedding light on their electrical conductivity and optoelectronic application potential. Dynamic stability was confirmed via phonon calculations, verifying the atomic-level stability of the compounds. Thermophysical analyses, including Debye temperature, melting temperature, and minimum thermal conductivity, were performed to assess the suitability of these compounds for high-temperature applications. Lastly, the optical properties were analyzed, focusing on parameters such as reflectivity, absorption, and optical conductivity, to explore the potential of these materials for use in optical devices or as coating materials.

This study aims to expand the limited literature data, especially on Mn_2N and Tc_2N compounds, by uncovering the unknown properties of these materials and providing guidance for future experimental and theoretical research. Moreover, it seeks to offer fundamental insights into the potential applications of X_2N compounds in advanced technological fields, such as energy storage, water splitting, and protective coatings.

Moreover, the utilization of the first-principles computational approach offers a potent means to investigate the physical and mechanical characteristics of materials. This study primarily investigates 2D hexagonal-type X_2N compounds using first-principles calculations. Our findings will offer a fundamental comprehension of these materials

and will be beneficial for future experimental and theoretical inquiries into this class of materials.

Methods

The properties of X_2N (X = Mn, Tc, and Re), including its structural, elastic, electronic, phonon, thermo-physical, and optical were computed using the Siesta package program with Density Functional Theory (DFT) [27]. The computations were executed utilizing a Generalized Gradient Approximation (GGA)-Perdew-Burke-Ernzerhof (PBE) exchange–correlation function [28]. Before starting the calculations, necessary geometry optimizations were performed. The most stable structures with minimum energy were obtained for the simulation study. And all calculations were performed on these structures. We utilized a Troullier-Martins norm-conserving pseudo-potential for the Mn, Tc, Re, and N atoms [29]. The valence electron configurations of the Mn, Tc, Re, and N atoms are $3d^5 4s^2, 4d^5 5s^2, 5d^5 6s^2,$ and$2s^2 2p^3$, respectively. All computations were performed using double-zeta plus polarized (DZP) basis sets consisting of localized atomic orbitals. The energy mesh cut-off, representing the distance between points in the real space grid used for calculating the Hartree, exchange, and correlation contributions to the total energy and Hamiltonian, was defined as 350 Rydberg (Ry). The Brillouin zones (BZ) were examined using a Monkhorst–Pack k-point mesh with dimensions of $10 \times 10 \times 4$ [30]. The conjugate-gradient (CG) technique was used to execute structural optimizations until the residual force acting on all atoms reached a value smaller than 0.01 eV/Å. Additionally, to examine each minimization step, we utilized the KPLOT program and the RGS method [31, 32], which provide comprehensive data on the space groups, atomic positions, and lattice parameters of the X_2N. Precise information on the material's hardness was obtained by calculating the Bulk modulus, Shear modulus, Young modulus, and Poisson's ratio. Using the volume-conserving approach, the Siesta program was utilized to estimate the second-order independent elastic constant values of X_2N. The hardness characteristics, including the Bulk modulus, Shear modulus, Young modulus, and Poisson's ratio, were calculated using the elastic constant values to obtain precise information on the material's hardness. The DFT method has proven to be one of the most accurate methods for the computation of the electronic structure of solids.

Results and discussions

Structural properties

The examination of structural characteristics is an essential step in the ab initio simulation analysis of materials, as it allows access to other physical properties such as electronic, optical, and elastic properties. For this analysis, we employed the GGA-PBE approximation to investigate the structural properties of X_2N (X = Mn, Tc, and Re) transition metal nitrides that correspond to space group #194 ($P6_3/mmc$). The primitive crystalline unit cell of X_2N (X = Mn, Tc, and Re) transition metal nitrides is depicted in Fig. 1. For the X_2N (X = Mn, Tc, and Re) compound, the X and N atoms occupy the following Wyckoff positions in the unit cell: X (4f) (0.33333, 0.66667, x) and N (2d) (0.33333, 0.66667, 0.75000). The unit cell contains four X atoms and two N atoms. The geometry optimization procedure was conducted under certain pressure and temperature conditions to investigate the properties of X_2N (X = Mn, Tc, and Re) in its lowest energy state. Table 1 displays the theoretical and experimental values for the structural properties. The calculated lattice constant values strongly agree with those obtained in previous studies [22, 33–35].

Elastic properties

The elastic qualities of a crystal material are closely associated with a variety of mechanical and physical aspects. The determination of elastic constants plays a crucial role in assessing the mechanical stability of a material, namely its capacity to withstand and respond to external stress. Crystals possessing a hexagonal structure represent five distinct elastic constants, namely C_{11}, C_{12}, C_{13}, C_{33}, and C_{44}. Table 2 displays the computed elastic values for X_2N compounds. For a hexagonal system to be considered mechanically stable, it must satisfy the following inequality criterion as outlined by the Born-Huang conditions [37]. $C_{11} > |C_{12}|$, $2C_{13}^2 < C_{33}(C_{11} + C_{12})$, $C_{44} > 0$. The compounds Mn_2N, Tc_2N, and Re_2N exhibit positive elastic constants and satisfy the mechanical stability criterion. This shows that X_2N compounds have mechanical stability based on Born-Huang criteria calculations.

C_{11} and C_{33} denote the linear compressive strength along the crystallographic directions [100] and [001], respectively. It is observed that the value of C_{33} is higher than that of C_{11} across all compounds. This finding suggests that in X_2N compounds, the bond strength is lower in the [100] direction compared to the [001] direction, and the compressibility is higher in the [100] direction compared to the [001] direction. In terms of compressibility, the order is

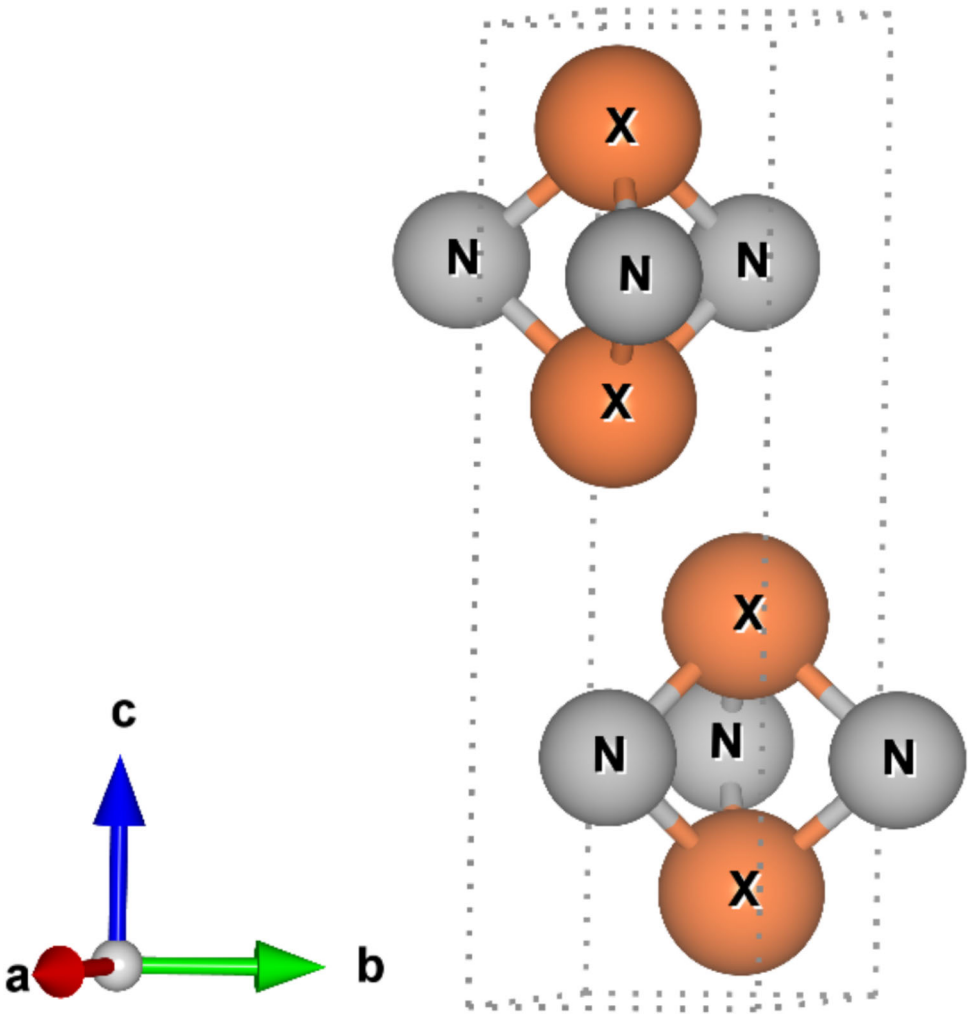

Fig. 1 Crystal Structure of X_2N compound

Table 1 Calculated equilibrium lattice parameter (in Å) for X_2N (X = Mn, Tc, and Re) compounds in comparison with available experimental data and previous theoretical results

Material	a	b	c	V	References
Mn_2N	2.627	2.627	8.867	52.99	This study
	2.620	2.620	8.840	26.37	[33]
Tc_2N	2.825	2.825	9.681	66.89	This study
	2.840	2.840	9.750	34.09	[33]
	2.800	2.800	9.660	32.79	[34]
Re_2N	2.851	2.851	9.835	69.20	This study
	2.857	2.857	9.877	34.91	[22]
	2.830	2.830	9.880	–	[35]
	2.837	2.837	9.799	–	[35]
	2.801	2.801	9.789	–	[33]
	2.860	2.860	9.870	34.89	[33]
	2.854	2.854	9.850	69.50	[36]

as follows: Tc_2N has more compressibility compared to Mn_2N, which in turn has greater compressibility than Re_2N.

The elastic constant C_{44} is utilized to quantify the compound's ability to withstand shear deformation under the influence of tangential stress exerted on the (100) plane in the [010] direction. The observed C_{44} value for X_2N is comparatively lower than the C_{11} and C_{33} values, suggesting that X_2N compounds exhibit more susceptibility to shear deformation rather than unidirectional stress along any of the three crystallographic orientations. As indicated in Table 2, the C_{44} and $C_{66} = (C_{11}–C_{12})/2$ values of X_2N compounds demonstrate that the C_{66} value for all compounds surpasses the C_{44} value. This implies that shearing along the (100) plane is comparatively more feasible than shearing along the (001) plane. Since $C_{11} + C_{12} > C_{33}$ for all compounds, it can be concluded that the bond in the (001) plane exhibits greater elastic stiffness compared to the bond along the c-axis and the elastic tensile modulus is higher in the (001) plane along the c-axis.

The parameter C' ($C' = \frac{C_{11}-C_{12}}{2}$) also known as the tetragonal shear modulus, is commonly employed in assessing the dynamical stability of a crystalline solid [40].

Table 2 Computed elastic constants, C_{ij} (in GPa), Cauchy pressure (C''), (in GPa), tetragonal shear modulus (C'), (in GPa), and Kleinman Parameter (ζ) of X_2N (X = Mn, Tc, and Re) compounds

Compound	C_{11}	C_{12}	C_{13}	C_{33}	C_{44}	C''	C'	ζ	References
Mn_2N	546.47	170.65	196.42	651.34	150.28	20.37	187.91	0.55	This Study
	559.00	162.00	200.00	659.00	157.00	–	–	–	[33]
Tc_2N	549.77	171.34	251.12	634.35	157.26	14.08	189.22	0.55	This Study
	550.00	182.00	261.00	653.00	154.00	–	–	–	[33]
	612.00	210.00	292.00	728.00	172.00	–	–	–	[34]
	499.00	159.00	278.00	564.00	147.00	–	–	–	[38]
Re_2N	676.00	209.25	264.98	808.30	183.44	25.80	233.38	0.54	This Study
	662.00	237.00	258.00	870.00	192.00	–	–	–	[39]
	642.00	201.00	295.00	767.00	171.00	–	–	–	[33]
	635.57	195.34	285.58	744.58	170.94	–	–	–	[36]

Also, it provides insight into the rigidity of a crystalline structure. In addition, it has been established that C' is intricately linked to the propagation of slow transverse acoustic waves and serves as a crucial factor in driving the structural modifications inside a given system [41]. The dynamical stability of a crystal is ensured when the value of C' is positive, while a negative value of C' signifies that the material is dynamically unstable. In Table 2, C' values for X_2N compounds are presented. It means that X_2N compounds are dynamically stable according to the presented C' value.

The Cauchy pressure, denoted as $C'' = C_{12}–C_{44}$, has been computed to elucidate the bonding characteristics of a compound at the atomic scale [42]. Materials exhibiting positive Cauchy pressure are commonly classified as ductile, whereas materials with negative values are indicative of brittleness [43]. According to Pettifor [44], materials with a large positive C'' value are characterized by robust metallic non-directional bonding. Conversely, materials having a low C'' value are associated with bonding that possesses an angular nature. The Cauchy pressure values obtained for X_2N are displayed in Table 2. The observation of a positive value for C'' for X_2N compounds indicates the presence of metallic bonding and the ductile behavior of the compound.

Polycrystalline elastic properties

The dimensionless Kleinman parameter (ζ) often ranges within the interval of 0 to 1, inclusive. Based on Kleinman's research [45], the lower boundary of ζ signifies a negligible influence of bond bending in countering external stress, whilst the upper boundary indicates a negligible impact of bond stretching or contracting in resisting externally applied stress. The Kleinman parameter is calculated by the following Eq. 1.

$$\zeta = \frac{C_{11} + 8C_{12}}{7C_{11} + 2C_{12}} \quad (1)$$

The calculated ζ value for the Mn_2N and Tc_2N compounds is 0.55 and for Re_2N is 0.56. From this, we can estimate that the mechanical strength in X_2N is mainly dominated by the bond bending contribution compared to that due to bond stretching or shrinkage.

The Voigt-Reuss-Hill (VRH) approach can be utilized to find the bulk modulus (B), shear modulus (G), Young's modulus (E), and Poisson's ratio (υ). The determination of the upper and lower bounds of the elastic moduli of polycrystalline materials is achieved through the application of the Voigt and Reuss approximations, respectively. The actual value lies within the range defined by the Voigt and Reuss limitations. The measure of a solid's resistance to compression induced by constant hydrostatic pressure is referred to as the bulk modulus (B) [46]. The shear modulus (G) [47] quantifies the ability of a solid to resist external stress that induces deformation. Young's modulus (E) is a physical property that quantifies the resistance of a solid material to changes in length under tensile stress [48]. The characteristic in question also plays a role in determining the stiffness of a solid. Based on the observed E values of the three compounds, it can be deduced that Re_2N exhibits more stiffness compared to Tc_2N and Mn_2N. The calculated values are displayed in Table 3. Based on the data presented in Table 3, it is evident that B is greater than G (B > G). This observation implies that the mechanical stability of X_2N (X = Mn, Tc, and Re) compounds is primarily governed by the shearing stress exerted on them. Furthermore, it can be inferred that the mechanical failure mechanism of X_2N (X = Mn, Tc, and Re) compounds is

Table 3 Calculated elastic moduli (all in GPa), Pugh's ratio, Young moduli (GPa), Poisson's ratio, and machinability index (μ^M) for the X_2N (X = Mn, Tc, and Re) compounds

Compound	B_R	B_V	B_H	G_R	G_V	G_H	E	B/G	υ	μ^M	References
Mn_2N	315.95	319.03	317.49	173.24	176.41	174.83	443.14	1.81	0.27	2.11	This study
Tc_2N	336.25	342.34	339.29	169.56	171.43	170.50	438.11	1.99	0.28	2.16	This study
	–	–	390.00	–	–	185.00	480.00	–	0.29	–	[34]
	321.00	333.00	327.00	144.00	149.00	147.00	384.00	–	0.30	–	[38]
Re_2N	398.85	404.30	401.57	211.06	214.79	212.93	542.84	1.89	0.27	2.19	This study
	416.80	411.10	413.90	212.70	215.40	214.00	547.70	1.93	0.27	2.16	[39]
	386.81	394.31	390.56	192.46	195.68	194.07	499.48	2.01	0.29	–	[36]

more susceptible to stress-induced changes in shape rather than pressure-induced changes in volume.

The computation of the bulk modulus (B) and shear modulus (G) was performed using Hill's [49] approximation, which is a method that calculates the average value between the upper limit (Voigt [50]) and lower limit (Reuss [51]). The mathematical expression for this approximation is as follows:

$$B_H = \frac{B_V + B_R}{2} \tag{2}$$

$$G_H = \frac{G_V + G_R}{2} \tag{3}$$

Using B and G, the following equations can be used to derive Young's modulus (E) and Poisson's ratio (Using B and G, the following equations can be used to derive Young's modulus E and Poisson's ratio (υ):

$$E = \frac{9GB}{(3B + G)} \tag{4}$$

$$\nu = \frac{(3B - 2G)}{2(3B + G)} \tag{5}$$

A solid is either brittle or ductile for most practical applications. The Pugh ratio (B/G), Poisson's ratio (ν), and Cauchy pressure (C'') are the three basic parameters that indicate the brittle and ductile characteristics of a system [39]. Pugh postulated an empirical correlation for discerning the contrasting characteristics of brittleness and ductility shown by various materials. The Pugh's ratio, also known as the ratio of the bulk and shear moduli (B/G), is a parameter that characterizes the ductility or brittleness of a certain material. The behavior of a material may be classified as ductile, or brittle based on the value of Pugh's ratio. It is well recognized that a material will exhibit ductile behavior when the Pugh's ratio exceeds 1.75, whereas it will demonstrate brittle behavior when the Pugh's ratio falls below 1.75 [52]. In the present study, the (B/G) values of 1.81, 1.99, and 1.89 have been determined for Mn_2N, Tc_2N, and Re_2N, respectively. These values indicate that the compounds are expected to have ductile characteristics. As can be seen in Table 3, it is consistent with the values in other studies.

The Poisson's ratio (ν) is a fundamental quantity utilized to characterize the extent of deformation, whether expansion or contraction, experienced by a material in the direction of applied stress. The parameter mentioned is also utilized to assess the resistance of solids to shear. The range of potential values for Poisson's ratio of a solid is constrained to the interval: $-1.0 \leq \nu \leq 0.5$ [17].

A value of ν equal to 0.5 means that elastic deformation has no effect on the volume [53]. The threshold value of this parameter, 0.26, predicts whether the material will be brittle or ductile. If the material is greater than 0.26, the material is ductile or if it is less than 0.26, it is brittle. Based on the data presented in Table 3, it is evident that Poisson's ratios of Mn_2N, Tc_2N, and Re_2N exceed the threshold value of 0.26. Consequently, it may be inferred that Mn_2N, Tc_2N, and Mn_2N exhibit ductility. This aligns with the findings of Pugh's ratio. A greater Poisson's ratio leads to better plasticity outcomes. The investigation of the value of ν [54, 55] enables the analysis of interatomic forces in solids. The predominance of central force interaction is observed when the aforementioned ratio remains within the range of 0.25 to 0.50. If the value is not in this range, it means that non-central forces are dominant. Therefore, in the compounds Mn_2N, Tc_2N, and Re_2N, the interatomic bonding is expected to be influenced by a central force.

The concept of machinability refers to the inherent characteristic of a material that determines the level of ease or difficulty in machining the material with a cutting tool. This characteristic is extensively utilized in the field of engineering for manufacturing and production purposes. The machinability of material is contingent upon many elements including the work material, the cutting tool employed, and the cutting parameters utilized. The

selection of cutting tool material, tool shape, cutting speed, cutting force, feed rate, and depth of cut is determined by the machinability of a material. Additionally, it plays a crucial role in determining the plasticity [56, 57] and dry lubricating characteristics of solid materials. The calculation for the machinability index (μ^M) of a material is as follows [58]:

$$\mu^M = \frac{B}{C_{44}} \tag{6}$$

Therefore, the combination of a strong bond and a low resistance to shear results in improved machinability and dry lubricity. Materials characterized by a high μ^M value exhibits exceptional lubricating characteristics, reduced feed forces, diminished friction values, and increased plastic strain values. Re_2N (2.19), in comparison to Mn_2N (2.11) and Tc_2N (2.16), possesses a greater μ^M. Additionally, the elastic moduli and rigidity constant of Re_2N are greater than those of Mn_2N and Tc_2N, confirming that Re_2N is more suitable for tool applications than Mn_2N and Tc_2N. Out of the phases under consideration, Re_2N exhibits the highest value (2.19) of μ^M, while Mn_2N demonstrates the lowest value.

Hardness

Hardness is a property of solids that quantifies their resistance to localized plastic deformation. In terms of the intended use, the hardness of the material is critical. A comprehension of the structural and mechanical reactions of a material under severe stress necessitates an understanding of the material's hardness. Solid hardness best indicators are considered to be C_{44} and G in terms of elastic constants and moduli [42, 59]. There exists a range of methodologies that may be employed to calculate the level of hardness in a given system. In this investigation, the hardness values were determined using the formalisms proposed by Teter et al. [60], Tian et al. [61], Miao et al. [62], Mazhnik et al. [63], and Chen et al. [64].

$$(H_V)_{miao} = \frac{(1-2\nu)\mathrm{E}}{6(1+\nu)} \tag{7}$$

$$(H_V)_{Chen} = 2\left[\left(\frac{G}{B}\right)^2 G\right]^{0.585} - 3 \tag{8}$$

$$(H_V)_{Tian} = 0.92(G/B)^{1.137} G^{0.708} \tag{9}$$

$$(H_V)_{Teter} = 0.151G \tag{10}$$

$$(H_V)_{Mazhnik} = \gamma_0 \chi(\sigma) E \tag{11}$$

$\chi(\sigma)$ in Eq. 11 is a function of the poison ratio and is calculated as follows:

$$\chi(\sigma) = \frac{1 - 8.5\sigma + 19.5\sigma^2}{1 - 7.5\sigma + 12.2\sigma^2 + 19.6\sigma^3}$$

Also, γ_0 is a dimensionless constant with a value of 0.096.

The $(H_V)_{miao}$, $(H_V)_{Chen}$, $(H_V)_{Tian}$, $(H_V)_{Teter}$, and $(H_V)_{Mazhnik}$ values obtained for the X_2N (X = Mn, Tc, and Re) compounds are presented in Table 4.

According to the hardness data calculated according to the hardness values shown in Table 4, the smallest hardness value among the three materials was obtained from $(H_V)_{Tian}$. According to the data provided in Table 4, the observed ranking of mean hardness levels achieved through various procedures is $Re_2N > Mn_2N > Tc_2N$. According to the $(H_V)_{Mazhnik}$ value only, the ranking was observed as $Re_2N > Tc_2N > Mn_2N$. Based on Chen's formula [64], it is determined that superhard materials possess a hardness value above 40 GPa. The calculated values of $(H_V)_{Chen}$ for Mn_2N, Tc_2N, and Re_2N are 17.41, 15.07, and 18.91 GPa, correspondingly. Therefore, it may be concluded that these materials do not possess an exceptionally high level of hardness.

Elastic anisotropy

The phenomenon of elastic anisotropy exerts influence on several mechanical processes, encompassing the development of plastic deformations inside crystalline structures, the propagation of fractures in materials, and the generation of cracks in materials. Anisotropic materials are characterized by their varying physical properties in different orientations. The comprehension of elastic anisotropy holds considerable implications for the fields of applied engineering sciences and crystal physics. Consequently, a comprehensive analysis of the elastic anisotropy characteristics for X_2N (X = Mn, Tc, and Re) compounds is crucial to gain a deeper understanding of their versatility and potential uses under various external stress conditions. Directional covalent bonding is a significant factor in influencing the anisotropy of crystals, whereas metallic bonding helps to enhance their overall isotropy [65]. The calculation of the Zener anisotropy factor (A) has been performed using the relation provided by Yang et al. [66].

Table 4 Calculated hardness (GPa) of X_2N (X = Mn, Tc, and Re) compounds

Compound	$(H_V)_{Chen}$	$(H_V)_{Tian}$	$(H_V)_{Teter}$	$(H_V)_{Miao}$	$(H_V)_{Mazhnik}$
Mn_2N	17.41	16.26	26.40	27.11	21.38
Tc_2N	15.07	14.17	25.75	24.46	22.09
Re_2N	18.91	17.79	32.15	31.98	26.68

$$A = \frac{2C_{44}}{C_{11} - C_{12}} \tag{12}$$

This parameter serves to quantify the degree of anisotropy shown by the elastic constants inside a single crystal. In the case of an isotropic crystal, the value of A is equal to 1. The measure of anisotropy is determined by the extent of deviation from unity. For Mn_2N, Tc_2N, and Re_2N, respectively, A = 0.800, 0.831, and 0.786, indicating that the compounds are anisotropic. The shear anisotropic factors have the potential to serve as a quantitative tool for assessing the level of anisotropy in atomic bonding across various crystal planes. The quantification of shear anisotropy in a hexagonal crystal can be achieved by the consideration of three distinct parameters [67, 68].

Shear anisotropy factor between ⟨011⟩ and ⟨010⟩ directions for shear plane {100},

$$A_1 = \frac{4C_{44}}{C_{11} + C_{33} - 2C_{13}} \tag{13}$$

Shear anisotropy factor between ⟨101⟩ and ⟨001⟩ directions for shear plane {010},

$$A_2 = \frac{4C_{55}}{C_{22}+C_{33}-2C_{23}} \tag{14}$$

Shear anisotropy factor between ⟨110⟩ and ⟨010⟩ directions for shear plane {001},

$$A_3 = \frac{4C_{66}}{C_{11}+C_{22}-2C_{12}} \tag{15}$$

The shear anisotropy factors of X_2N (X = Mn, Tc, and Re) have been determined and are presented in Table 5. When the crystal is isotropic, all three variables have a value of 1. In the case of alternative values, the crystal exhibits anisotropic properties. According to the calculated values of A_1 and A_2, it may be inferred that the compounds exhibit a considerable level of anisotropy. However, the value of A_3 suggests isotropy. For a hexagonal structure, $C_{11} = C_{22}$, $C_{44} = C_{55}$, and $C_{13} = C_{23}$, therefore $A_1 = A_2$.

Table 5 Elastic anisotropy indices of X_2N (X = Mn, Tc, and Re) compounds

Parameters	Mn_2N	Tc_2N	Re_2N
A	0.800	0.831	0.786
A_1	0.747	0.922	0.769
A_2	0.747	0.922	0.769
A_3	1.000	1.000	1.000
A_B	0.005	0.009	0.007
A_G	0.009	0.005	0.009
A^U	0.101	0.073	0.102
d_E	2.470	2.464	2.470
A^{eq}	1.336	1.280	1.337
A^L	0.080	0.057	0.093
K_c/K_a	0.713	0.571	0.654

Solids of any crystal symmetry can have their universal anisotropy index (A^U and d_E), equivalent Zener anisotropy measure (A^{eq}), anisotropy in shear (A^G), and anisotropy in compressibility (A^B) evaluated using the following standard formulae [69–73].

$$A^U = \frac{B_V}{B_R} + 5\frac{G_V}{G_R} - 6 \geq 0 \tag{16}$$

$$d_E = \sqrt{A^U + 6} \tag{17}$$

$$A^{eq} = \left(1 + \frac{5}{12}A^U\right) + \sqrt{\left(1 + \frac{5}{12}A^U\right)^2 - 1} \tag{18}$$

$$A_B = \frac{B_V - B_R}{B_V + B_R} \tag{19}$$

$$A_G = \frac{G_V - G_R}{G_V + G_R} \tag{20}$$

The Universal Anisotropy Index (A^U) is a commonly utilized metric for quantifying anisotropy in elastic characteristics. The measure of anisotropy discussed here is independent of crystal symmetry. The parameter A^U is unique among current anisotropy metrics since it incorporates contributions from both shear and bulk effects. Based on Eq. (16), it can be inferred that the ratio G_V/G_R exerts a more significant impact on the anisotropy index A^U compared to the ratio B_V/B_R. The anisotropy index is equal to zero in the case of an isotropic material. However, if the A^U value is smaller or larger than zero, it indicates the presence of various levels of anisotropy. The computed A^U values for Mn_2N, Tc_2N, and Re_2N are determined to be 0.101, 0.073, and 0,102, respectively, indicating the presence of anisotropic characteristics. When the Zener anisotropy measure value has a value of 1, the materials represent isotropy; any value other than 1 indicates anisotropy of the materials.

The A^{eq} values calculated for the compounds X_2N (X = Mn, Tc, and Re) are presented in Table 5. According to the values in Table 5, it can be said that these compounds are moderately anisotropic. A_B and A_G values take values ranging between 0 and 1. While A_B and A_G values of 1 represent maximum elastic anisotropy, A_B and A_G values of 0 represent perfect elastic isotropy. As can be seen from the A_B and A_G values presented in Table 5, for Mn_2N and Re_2N compounds, the fact that the A_G value is greater than the A_B value means that the shear anisotropy is greater than the compressibility anisotropy, but for Tc_2N compound, the A_B value is greater than the A_G value

indicates that the compressibility anisotropy is greater than the shear anisotropy.

The universal log-Euclidean anisotropy index is defined as follows [66–68].

$$A^L = \sqrt{\left[\ln\left(\frac{B_V}{B_R}\right)\right]^2 + 5\left[\ln\left(\frac{C_{44}^V}{C_{44}^R}\right)\right]^2} \quad (21)$$

The constants $C_{44}^V = \frac{3}{5}\frac{(C_{11}-C_{12}-2C_{44})}{3(C_{11}-C_{12})+4C_{44}}$ and $C_{44}^R = \frac{5}{3}\frac{C_{44}(C_{11}-C_{12})}{3(C_{11}-C_{12})+4C_{44}}$ are the Voigt and Reuss approximations for the elastic constant C_{44}, respectively. Like the universal anisotropy index, the A^L expression applies to crystal symmetry of any kind. Ensuring accurate scaling to account for perfect isotropy, this index remains valid across all crystallographic point symmetry groups. In contrast, when extremely anisotropic crystallites are considered, A^L is less sparse than A^U, making it a more suitable option for the current analysis. Simply the anisotropic nature of A^U is insufficient to account for the absolute magnitude of anisotropy [65]. Therefore, the utilization of A^L computation, which involves the comparison of the average stiffness values C^V and C^R, is seen to be a more suitable approach for investigating anisotropy. The values of A^L range from a minimum of 0 to a maximum of 10.26, and greater than 1 for almost 90% of solids. For perfect isotropy, A^L is equal to zero. Mn_2N, Tc_2N, and Re_2N have A^L values equal to 0.08, 0.057, and 0.093 respectively, these values are less than 1, indicating that the calculated compounds have moderate anisotropy. It has been claimed that materials with higher A^L values have a layered structure, while materials with lower A^L values have a non-layered structure[69, 74, 75]. The relatively low value of A^L suggests that X_2N (X = Mn, Tc, and Re) lacks a pronounced layered characteristic.

The calculation of linear compressibility along the a and c axes is determined using the subsequent equation [76]:

$$\frac{k_c}{k_a} = f = \frac{C_{11} + C_{12} - 2C_{13}}{C_{33} - C_{13}} \quad (22)$$

The f value is a crucial parameter that determines the isotropic or anisotropic nature of a material. Specifically, if the f value is equal to 1, the material can be classified as isotropic. However, if the f value deviates from 1, it indicates that the material is anisotropic. Based on the data provided in Table 6, it can be observed that the X_2N (X = Mn, Tc, and Re) compounds exhibit anisotropic behavior. The results presented in Table 5 are unique and do not have any existing estimates available for comparison.

The bulk modulus along the a, b, and c axes and its anisotropies are defined by the following equations [67].

$$B_a = a\frac{dP}{da} = \frac{\Lambda}{1+\alpha+\beta} \quad (23)$$

$$B_b = b\frac{dP}{db} = \frac{B_a}{\alpha} \quad (24)$$

$$B_c = c\frac{dP}{dc} = \frac{B_a}{\beta} \quad (25)$$

$$B_{relax} = \frac{\Lambda}{(1+\alpha+\beta)^2} \quad (26)$$

where

$$\Lambda = C_{11} + 2C_{12}\alpha + C_{22}\alpha^2 + 2C_{13}\beta + C_{33}\beta^2 + 2C_{23}\alpha\beta$$

and

$$\alpha = \frac{\{(C_{11}-C_{12})(C_{33}-C_{13})\} - \{(C_{23}-C_{13})(C_{11}-C_{13})}{\{(C_{33}-C_{13})(C_{22}-C_{12})\} - \{(C_{13}-C_{23})(C_{12}-C_{23})\}}$$

$$\beta = \frac{\{(C_{22}-C_{12})(C_{11}-C_{13})\} - \{(C_{11}-C_{12})(C_{23}-C_{12})\}}{\{(C_{22}-C_{12})(C_{33}-C_{13})\} - \{(C_{12}-C_{23})(C_{13}-C_{23})\}}$$

The parameter denoted as B_{relax} represents the bulk modulus of an isotropic single crystal. The value of the entity is equivalent to the value derived from the Reuss approximation. The magnitudes of B_a and B_b are significantly less than those of B_c. According to the findings, X_2N (X = Mn, Tc, and Re) exhibits lower compressibility when subjected to stress along the c-direction compared to stress along the a-direction or b-direction. The data in Table 6 are novel and lack any existing comparative data in the literature.

$$A_{B_a} = \frac{B_a}{B_b} \quad (27)$$

$$A_{B_c} = \frac{B_c}{B_b} \quad (28)$$

Based on the data provided in Table 6, it can be observed that the value of A_{B_a} is equal to 1 for X_2N compounds, indicating isotropy in the axial bulk modulus. However, A_{B_c} is not equal to 1, suggesting the presence of anisotropy in the axial bulk modulus. The bulk modulus along the c-axis is more than that along the a- and b-axes. In addition, it is worth noting that the values of the uniaxial bulk modulus are distinct and significantly greater than the values of the isotropic bulk modulus.

To conduct a more comprehensive examination of the anisotropic properties displayed by the compounds under investigation, we have utilized three-dimensional (3D) plots. The plots were obtained by employing the VELAS code [77]. In addition, an in-depth analysis of the elastic characteristics, namely Young's modulus (E), linear compressibility, shear modulus (G), and Poisson's ratio (υ), has been incorporated in Table 7, including their respective lower and upper limits. The presented table offers a

Table 6 Bulk modulus (B_{relax} in GPa), bulk modulus along a, b, and c-axes (B_a, B_b, and B_c in GPa), and α and β of X_2N (X = Mn, Tc, and Re) compounds

Compound	B_{relax}	B_a	B_b	B_c	α	β	A_{B_a}	A_{B_c}
Mn_2N	315.95	857.13	857.13	1202.44	1.00	0.71	1.00	1.403
Tc_2N	336.25	864.53	864.53	1513.71	1.00	0.57	1.00	1.750
Re_2N	398.85	1058.54	1058.54	1618.68	1.00	0.65	1.00	1.529

comprehensive summary of the elastic properties of the examined materials, facilitating efficient comparisons among various compositions. Figure 2 only presents the 3D diagrams of the Mn_2N, Tc_2N, and Re_2N compounds. When the plot assumes a spherical (3D) form, it signifies a state of complete isotropy in three dimensions. In contrast, deviations from a spherical configuration can be considered indicators of the degree of anisotropy present in different orientations across the three-dimensional domain. The Young's modulus (E), shear modulus (G), and Poisson's ratio (υ) of materials exhibit significant anisotropy in all the planes.

Electronic band structure and density of states

The calculation of the electronic band structure aids in the comprehension of numerous physical properties exhibited by crystalline solids. The band structure provides a near-complete explanation for both optical and charge transport characteristics. As depicted in Figs. 3, 4 and 5, we have computed the electronic band structure ($E–E_F$) of X_2N (X = Mn, Tc, and Re) along high symmetry directions (Γ–M–K–Γ–A–L–H) within the k-space. The Fermi energy level is shown as a red horizontal dashed line (Figs. 3, 4 and 5). Due to the evident overlapping of conduction and valence bands at the Fermi level, the band structure of X_2N (X = Mn, Tc, and Re) suggests that it is metallic. The dispersion of the bands traversing the Fermi level exhibits considerable variation across different regions of the k-space. There is a crossing of the Fermi level by both electron-like and hole-like bands. When bands are highly dispersive, it indicates that the charge carrier effective mass is low and that charge mobility is high. When it comes to non-dispersive bands, the situation is completely different.

Figures 3, 4 and 5 display the computed total and partial density of states (PDOS) for X_2N (X = Mn, Tc, and Re) compounds as a function of energy ($E-E_F$). The Fermi level, E_F, is indicated by a vertical dashed line at 0 eV. To determine the individual impact of each atom on the Total Density of States (TDOS), we have computed the Partial Density of States (PDOS) for both the X (X = Mn, Tc, and Re) and N atoms in X_2N. The presence of non-zero values of the total density of states at the Fermi level provides evidence that X_2N is expected to display metallic electrical conductivity. The dominant contribution to the total density of states in the vicinity of the Fermi level arises from the d orbitals and N-p orbitals of all compounds. Therefore, these electronic states have a significant influence on the electrical conductivity and other transport factors of X_2N. The peaks in the total density of states exert a significant influence over the compound's optoelectronic capabilities, which are dependent on energy. The stability of X_2N is influenced by the bonding electronic states of X-d and N-2p orbitals, as well as its structural, electrical, and mechanical properties. The peak closest to the negative energy below the Fermi level in TDOS is referred to as the bonding peak, whereas the peak closest to the positive energy is called the anti-bonding peak. The energy difference between these peaks is referred to as the pseudo-gap, which serves as an indicator of electrical stability [78, 79].

Vibrational properties

The characteristics of phonons play a crucial role in the field of solid-state physics. Phonon dynamics have an impact on all factors related to thermal and charge transfer. The characteristics of the phonon modes determine the dynamic and structural stability of a crystal. Phonon dispersion spectra can be used to measure several characteristics of a material directly or indirectly [80]. Phonon dispersion curves serve as important instruments for clarifying the dynamical stability of materials, unveiling structural phase transitions, and comprehending the intricate interplay between atomic vibrations and thermal properties [81]. In this study, the dynamical stability of the X_2N (X = Mn, Tc, and Re) compounds was investigated by analyzing the phonon dispersion curves at absolute zero temperature. The computational analysis was conducted utilizing the finite displacement technique, which is rooted in the principles of density functional perturbation theory (DFPT) [82]. Figure 6, 7 and 8 illustrates the phonon dispersion spectra of the aforementioned materials along the high symmetry direction of the Brillouin zone. The phonon dispersion curves do not show any negative frequency branch within the Brillion region for all compounds. This

Table 7 The minimum and maximum values of Young's modulus (GPa), compressibility (TPa^{-1}), shear modulus (GPa), Poisson's ratio, and their ratios for X_2N (X = Mn, Tc, and Re)

Compound	E_{min}	E_{max}	A_E	β_{min}	β_{max}	A_β	G_{min}	G_{max}	A_G	υ_{min}	υ_{max}	A_υ
Mn_2N	411.66	543.74	1.32	0.83	1.67	1.40	150.27	199.51	1.33	0.20	0.38	1.85
Tc_2N	428.95	459.46	1.07	0.66	1.57	1.75	157.26	189.22	1.20	0.16	0.37	2.31
Re_2N	507.08	649.67	1.28	0.62	0.95	1.53	183.44	236.15	1.29	0.20	0.39	1.94

indicates that the compounds considered in this study are dynamically stable. The maximum vibrational frequency manifests in the vicinity of the M-point within the Brillouin zone. The calculated phonon dispersion curve can be categorized into two sections, which include acoustic modes and optical modes. The optical behavior is highly influenced by the optical branches located at the upper part of the phonon dispersive curve. Furthermore, phonon dispersion curves can provide additional information. Six atoms are present in the unit cells of the investigated compounds. These atoms contribute to a total of 18 vibrational modes in the phonon dispersion curves. Three of these vibrational modes are acoustic modes and the remaining fifteen are optical modes.

Thermo-physical properties

The Debye temperature (θ_D) is a crucial thermophysical characteristic in crystals that is associated with various physical properties, including melting temperature, coefficient of thermal expansion, thermal conductivity, lattice vibration, interatomic bonding, and phonon specific heat. The temperature at which the activation of all atomic vibration modes occurs is known as the Debye temperature. Only acoustic modes can produce vibrational excitations at low temperatures. The Debye temperature is the threshold temperature at which all atomic vibrational modes become engaged. At low temperatures, the only cause of vibrational excitations is acoustic modes. Consequently, the value of θ_D obtained from the elastic constants and specific heat is the same at low temperatures. The temperature of this system is contingent upon the rigidity of the crystal and the masses of the individual atoms that make up the compound. In general, materials with stronger interatomic bonding, higher melting temperature, greater hardness, higher mechanical wave velocity, and lower average atomic mass tend to have bigger Debye temperatures. Using crystal density (ρ) and average speed of sound (v_m), we estimated the θ_D from the following equation [83]:

$$\theta_D = \frac{h}{k_B}\left[\left(\frac{3N}{4\pi}\right)\frac{N_A\rho}{M}\right]^{\frac{1}{3}} v_m \tag{29}$$

The Planck's constant (h), Boltzmann constant (k), Avogadro's number (N_A), density (ρ), molecular weight (M), number of atoms (N), and mean sound velocity (v_m) are all variables in this equation. It is evident from the given equation that θ_D is directly proportional to the mean sound velocity (v_m), which is dependent on the elastic characteristics of a crystal. The value of v_m can be determined by using the bulk modulus (B), shear modulus (G), longitudinal sound velocity (v_l), and transverse sound velocity (v_t) according to the equations provided in reference [84].

$$v_m = \left[\frac{1}{3}\left(\frac{2}{v_t^3} + \frac{1}{v_l^3}\right)\right]^{-\frac{1}{3}} \tag{30}$$

where,

$$v_t = \sqrt{\frac{G}{\rho}} \tag{31}$$

$$v_l = \sqrt{\frac{3B + 4G}{3\rho}} \tag{32}$$

θ_D, v_m, v_l, v_t and ρ calculated for X_2N (Mn, Tc, and Re) compounds are given in Table 8.

Higher values of the Debye temperature are known to imply stronger chemical bonds and higher phonon thermal conductivity. Table 8 shows that the Debye temperatures for Mn_2N, Tc_2N, and Re_2N are 760.24, 601.79, and 497.10 K, respectively. The Debye temperature of Mn_2N is higher than Tc_2N and Re_2N, suggesting that Mn_2N has stronger chemical bonds and higher phonon thermal conductivity.

A key aspect in determining the suitability of a material for usage is understanding its temperature threshold, which may be determined by the study of its melting temperature (T_m). The melting temperatures of crystalline materials are connected with their thermal expansion, elastic constants, and bonding energy. Materials possessing elevated melting temperatures exhibit enhanced atomic bonding strength

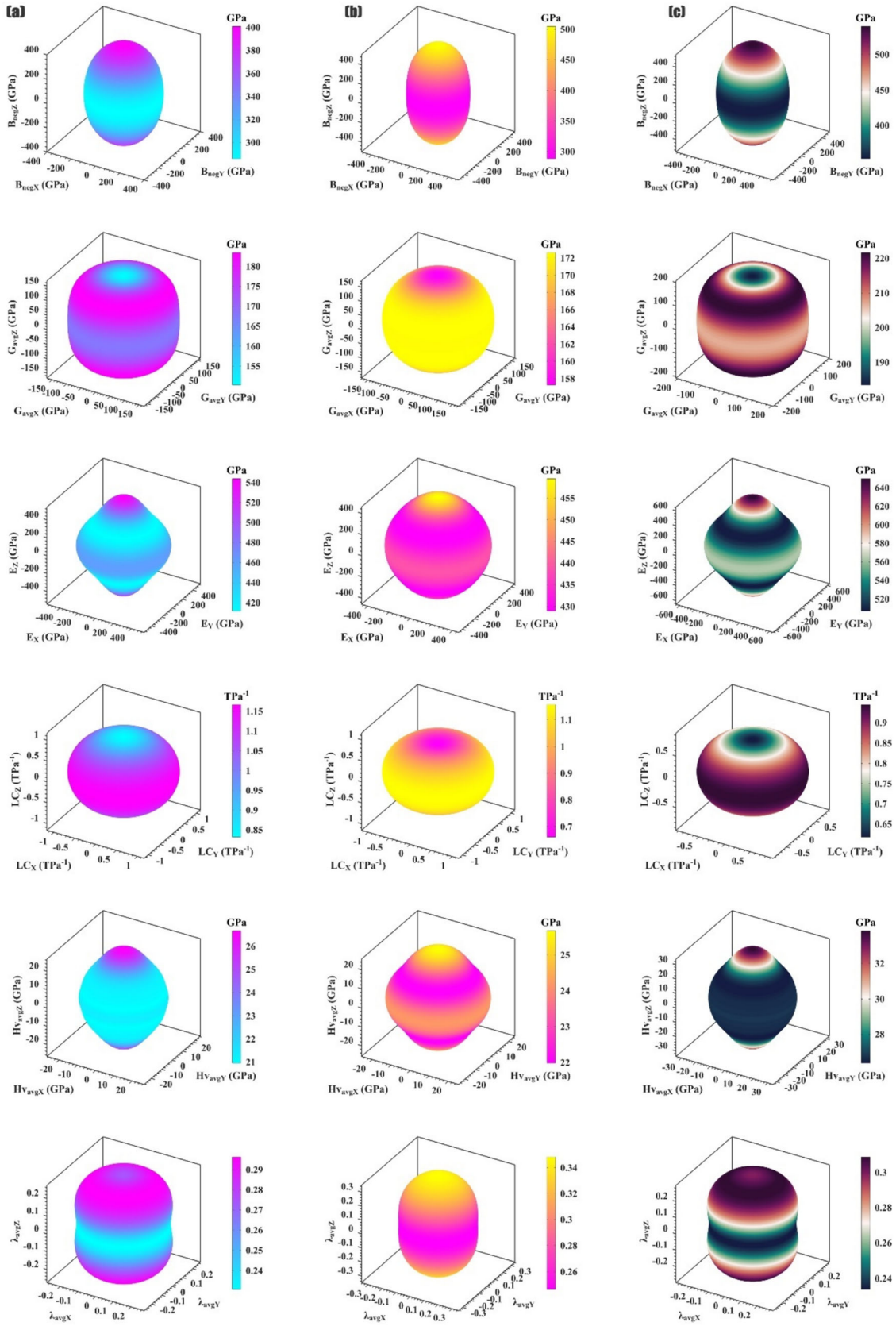

Fig. 2 3D directional dependences of Bulk modulus, Shear modulus, Young modulus, linear compressibility, hardness, and Poisson's ratio for (**a**) Mn_2N, (**b**) Tc_2N, and (**c**) Re_2N

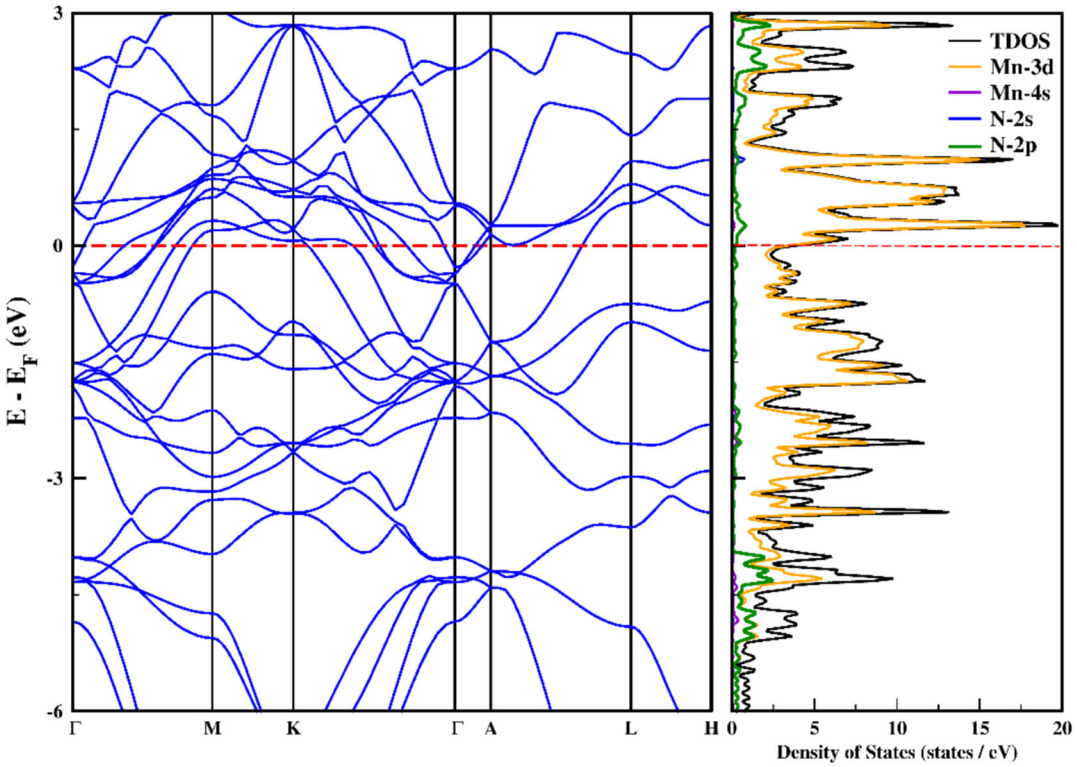

Fig. 3 Energy band structure and density of states of the Mn_2N compound

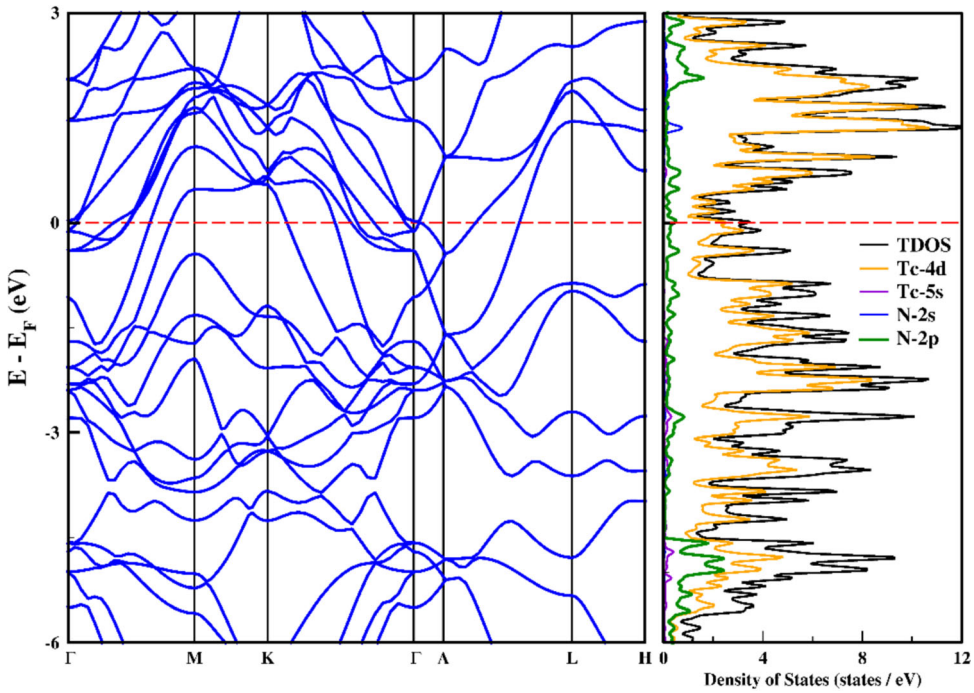

Fig. 4 Energy band structure and density of states of the Tc_2N compound

and reduced coefficient of thermal expansion. Knowledge of a material's melting point also aids in determining the temperature at which it can be used continuously without experiencing oxidation, chemical changes, or undue heating-related deformation [85]. The following formula can be used to determine the melting temperature (T_m) of materials using the elastic constants [86].

$$T_m = 354 + 1.5(2C_{11} + C_{33}) \quad (33)$$

Table 8 shows the estimated melting temperature of

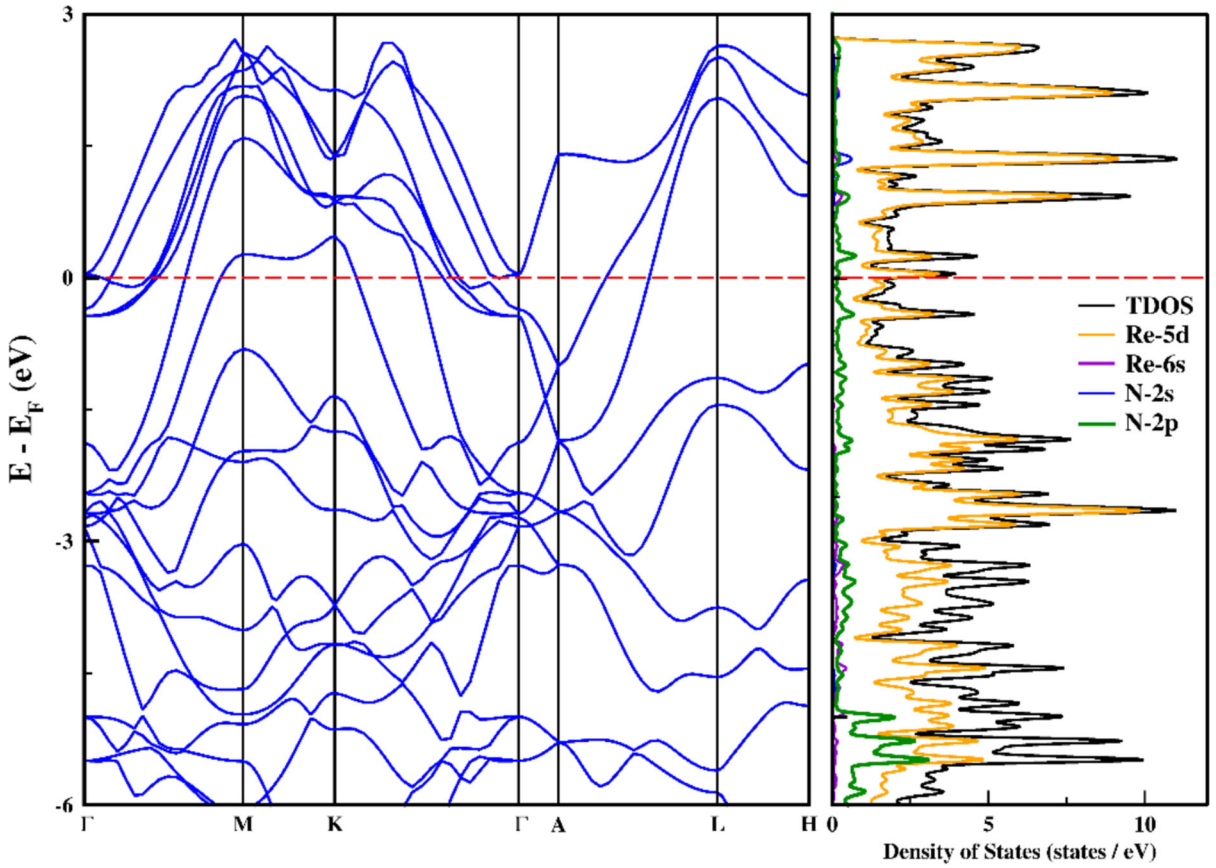

Fig. 5 Energy band structure and density of states of the Re_2N compound

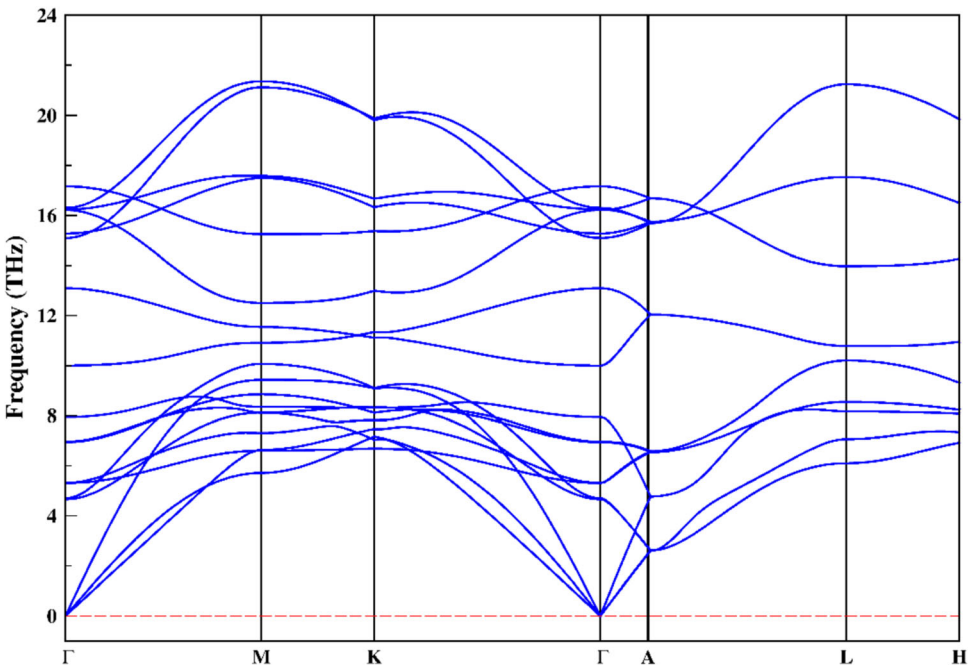

Fig. 6 Phonon dispersions of the Mn_2N compound

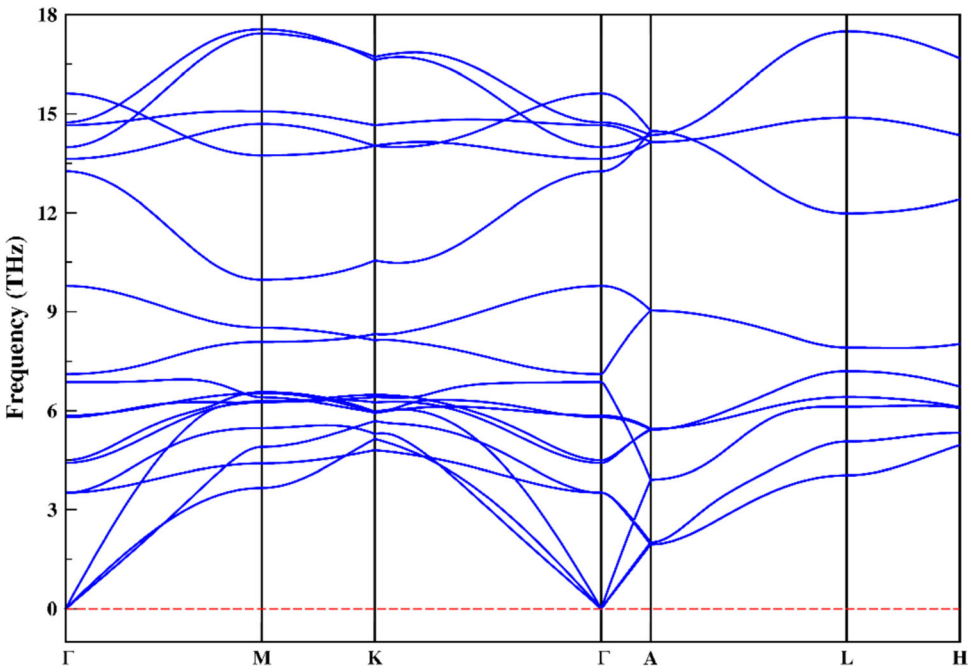

Fig. 7 Phonon dispersions of the Tc_2N compound

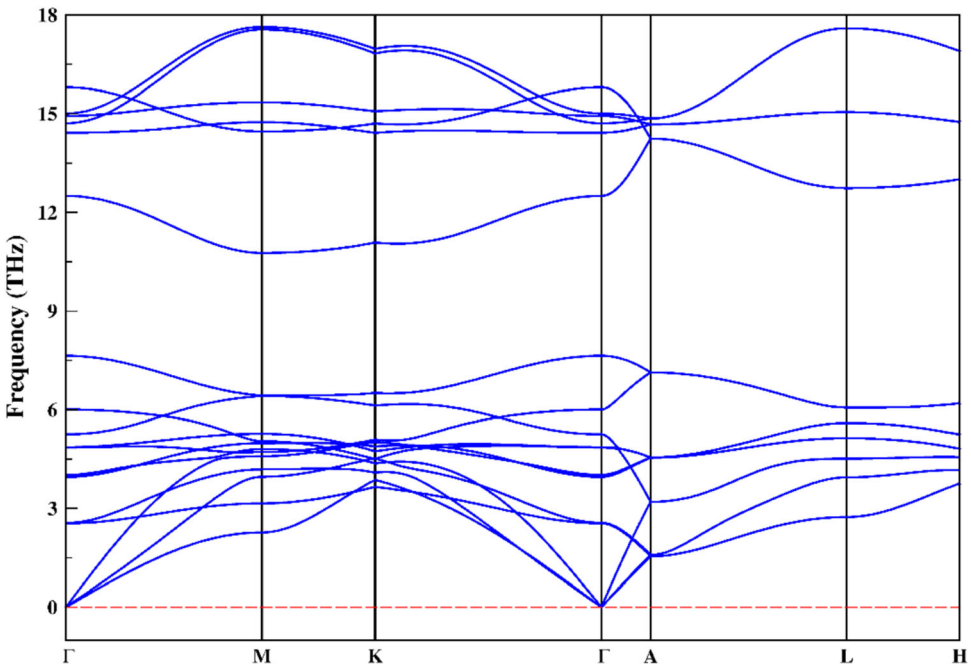

Fig. 8 Phonon dispersions of the Re_2N compound

X_2N (X = Mn, Tc, and Re). Re_2N has a greater melting temperature than Mn_2N and Tc_2N, indicating that it is a better suitable material for high-temperature applications than Mn_2N and Tc_2N.

For many applications it is important to describe the ability of a material to conduct heat energy. K_{min}, the minimum thermal conductivity, is a crucial parameter for the high-temperature application of materials. Equation 34 [87] was used to calculate K_{min}. The values obtained are shown in Table 8.

$$K_{min} = k_B v_m \left(\frac{M}{n\rho N_A} \right)^{-\frac{2}{3}} \tag{34}$$

For Mn_2N, 1.71, for Tc_2N, 1.25, and for Re_2N, 1.02 W m^{-1} K^{-1} were obtained. The value obtained for Mn_2N was larger than Tc_2N and Re_2N. This suggests that Mn_2N may be more suitable for high-temperature applications.

An important parameter that determines anharmonic effects in a crystal is the Grüneisen parameter. The Grüneisen parameter, denoted as γ, is a significant quantity in

Table 8 Calculated mass density (ρ in g/cm^3), longitudinal, transverse, and sound velocities (v_l, v_t, and v_m in m s^{-1}, respectively), Debye temperature (θ_D in K), melting temperature (T_m in K), and minimum thermal conductivity (K_{min} in Wm^{-1} K^{-1}) of X_2N (X = Mn, Tc, and Re)

Compound	ρ	v_t	v_l	v_m	T_m	θ_D	K_{min}	γ
Mn_2N	7.76	4745.27	8421.17	5279.03	2970.41	760.24	1.71	1.59
Tc_2N	10.31	4065.22	7410.90	4532.12	2954.85	601.79	1.25	1.68
Re_2N	18.54	3388.55	6079.88	3773.05	3594.47	497.10	1.02	1.63

the fields of thermodynamics and lattice dynamics due to its association with the heat capacity, bulk modulus, volume of a solid, and thermal expansion coefficient. The higher the value of the Grüneisen parameter, the higher the harmonicity. Using Poisson's ratio, the Grüneisen parameter is calculated from the following equation [88].

$$\gamma = \frac{3(1+v)}{2(2-3v)} \tag{35}$$

A high value of the Grüneisen parameter results in a high coefficient of thermal expansion and high crystal compressibility. Table 8 shows the calculated Grüneisen parameter values for X_2N (X = Mn, Tc, and Re) compounds. The Grüneisen parameter of the Tc_2N (1.68) compound is larger than that of the Re_2N (1.63) and Mn_2N (1.59) compounds, respectively. This means that the Tc_2N compound has higher crystalline compressibility and a higher coefficient of thermal expansion than the other calculated compounds.

Optical properties

A comprehensive comprehension of the optical characteristics of materials is crucial for the progress of optical technology and its applications. The underlying electronic band structure of the system of interest governs all the significant optical properties that depend on photon energy. This section provides a comprehensive presentation of the detailed computations of optical characteristics. The reflectivity, optical conductivity, and absorption were derived by calculating the complex dielectric constants of X_2N (X = Mn, Tc, and Re). The optical spectrum mechanism arises from the complex dielectric functions. $(\omega) = \varepsilon_1(\omega) + i\varepsilon_2(\omega)$ where ε_1 and ε_2 are the real and imaginary terms, respectively. The real portion $\varepsilon_1(\omega)$ is obtained through the application of Kramer–Kronig transformations [89] to $\varepsilon_2(\omega)$.

$$\varepsilon_1(\omega) = 1 + \frac{2}{\pi}\int_0^{\infty} \frac{\varepsilon(\omega\prime)\omega' \mathrm{d}\omega'}{\omega'^2 - \omega^2} \tag{36}$$

Figures 9(a–c) display the real (Re) and imaginary part (Im) spectra of the dielectric function for X_2N (X = Mn, Tc, and Re) compounds.

The imaginary part of the dielectric function is related to dielectric losses. Figures 9(a–c) show that the real part of the dielectric function crosses zero from the negative part at about 15 eV, whereas the imaginary part flattens out at a very low value at the same energy levels, indicating that the material will exhibit transparency for photons with energies exceeding 15 eV. The observation validates specifically the metallic properties of X_2N (X = Mn, Tc, and Re).

Reflectivity, R(ω), quantifies the proportion of the energy of the incident light that is reflected by the material. The R(ω) spectrum of the X_2N (X = Mn, Tc, and Re) compound is illustrated in Fig. 9(d). X_2N (X = Mn, Tc, and Re) compounds are observed to be very good reflectors in the infrared and visible light regions. Li et al. [90] state that a compound can effectively reduce solar heating if it has a reflectivity of approximately 44% in the visible light range. Thus, X_2N (X = Mn, Tc, and Re) compounds exhibit great potential as a coating material for mitigating solar heating.

The absorption coefficient is a significant optical parameter that gives essential information about the absorption of optical energy over a given distance. Optical absorption occurs when the frequency of an incoming photon resonates with the transition frequency of an atom. Due to the frequency dependence of the absorption coefficient, the materials can only absorb photons of a given frequency. Optical absorption occurs when electrons shift from occupied states in the upper valence band to unoccupied accessible states in the lower conduction band. Photon absorption is reported to commence at zero energy for X_2N (X = Mn, Tc, and Re) compounds. Therefore, no optical band gap is observed. It is also an indication of the conductivity of X_2N (X = Mn, Tc, and Re) compounds. The X_2N (X = Mn, Tc, and Re) compounds exhibit maximal absorption peaks within the photon energy range of 5 − 11 eV, suggesting their suitability as efficient absorbing materials in the ultraviolet region. The highest values of the absorptions were obtained as 8.85 eV, 9.05 eV, and 10.15 eV for Mn_2N, Tc_2N, and Re_2N,

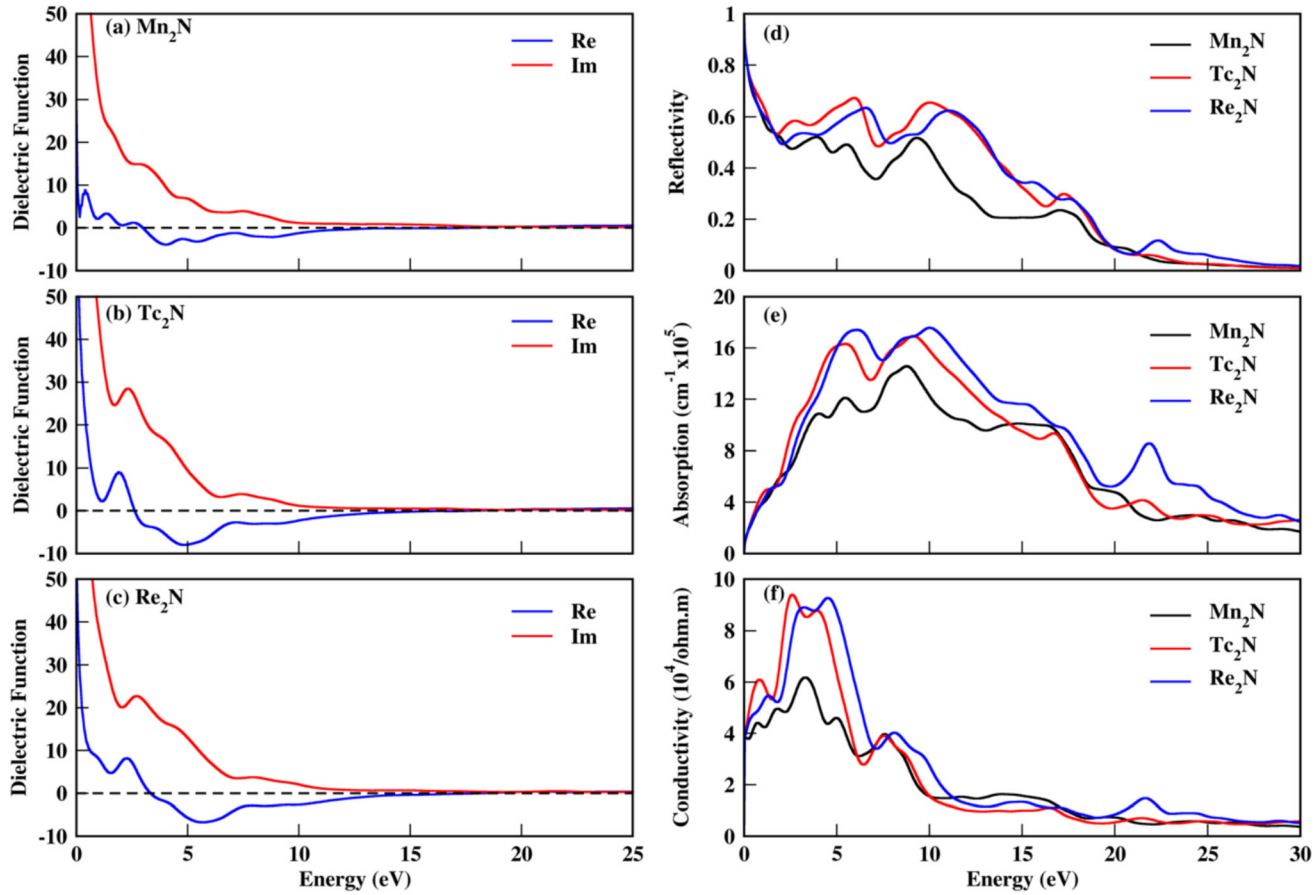

Fig. 9 Real and imaginary parts of the dielectric function, reflectivity, absorption and conductivity of X_2N (X = Mn, Tc, and Re) compound

respectively. The curves representing the absorption coefficient are displayed in Fig. 9(e).

The spectrum of optical conductivity is illustrated in Fig. 9(f). The material's optical conductivity commences at zero photon energy, suggesting the absence of a band gap, as confirmed by calculations of the material's band structure and density of states (Figs. 3, 4 and 5). For X_2N (X = Mn, Tc, and Re) compounds, it reaches maximum conductivity at 3.45 eV, 2.72 eV, and 4.69 eV, respectively, starts to decrease with further increase in energy, and approaches zero after about 30 eV. The highest optical conductivity value is observed in the Tc_2N compound, while the lowest optical conductivity is observed in the Mn_2N compound.

Conclusion

The physical characteristics of the hexagonal structures of the X_2N compound were computed using density functional theory. The geometry optimization yielded lattice parameter values that closely matched those reported in the literature. Since the valence band and conduction band cross each other around the Fermi energy level, all three structures have metallic properties. To obtain information about the stability of the X_2N compound, its elastic and vibration properties were examined. From the calculations, it was seen that all three compounds were stable both mechanically and dynamically. According to the bulk modulus, Shear modulus, and Poisson's ratio values obtained using the second-order elastic constant values, X_2N compounds have ductile properties in a hexagonal structure. Additionally, in these compounds, atoms are connected to each other by ionic bonds. Furthermore, the thermo-physical properties of the compounds were examined. Debye temperatures for Mn_2N, Tc_2N, and Re_2N are obtained as 760.24 K, 601.79 K, and 497.10 K, respectively. Additionally, the optical characteristics of the X_2N compound, including conductivity, reflectivity, and absorption coefficient, were examined.

Acknowledgements This study was supported by the Osmaniye Korkut Ata University under Scientific Research Project (BAP) No: OKÜBAP-2023-PT1-005

Funding Open access funding provided by the Scientific and Technological Research Council of Türkiye (TÜBİTAK).Open

References

[1] B Gao, X Li, K Ding, C Huang, Q Li, P K Chu and K Huo *J. Mater. Chem. A* **7** 14 (2019)
[2] Y Hinuma, T Hatakeyama, Y Kumagai, L A Burton, H Sato, Y Muraba, S Iimura, H Hiramatsu, I Tanaka and H Hosono *Nat. Commun.* **7** 11962 (2016)
[3] X Peng, C Pi, X Zhang, S Li, K Huo and P K Chu *Energy Fuels* **3** 366 (2019)
[4] O Volnianska and P Bogusławski *Phys. Rev. B—Condensed Matter Matter.* **75** 224 (2007)
[5] S R Römer, T Dörfler, P Kroll and W Schnick *Phys. Status Solidi B* **246** 1604 (2009)
[6] J Serrano, A Rubio, E Hernández, A Muñoz and A Mujica *Phys. Rev. B* **62** 16612 (2000)
[7] Y Zhong, X Xia, F Shi, J Zhan, J Tu and H J Fan *Adv. Sci.* **3** 1500286 (2016)
[8] Y Abghoui and E Skúlason *J. Phys. Chem. C* **121** 24036 (2017)
[9] J Luo, X Tian, J Zeng, Y Li, H Song and S Liao *ACS Catal.* **6** 6165 (2016)
[10] Y Abghoui and E Skúlason *Catal. Today* **286** 69 (2017)
[11] L Huang, Z Hu, H Jin, J Wu, K Liu, Z Xu, J Wan, H Zhou, J Duan and B Hu *Adv. Funct. Mater.* **30** 1908486 (2020)
[12] S Yuan, S-Y Pang and J Hao. *Appl. Phys. Rev.* **7** (2020)
[13] Y Zheng, X Li, C Pi, H Song, B Gao, P K Chu and K Huo *FlatChem* **19** 100149 (2020)
[14] C L Freeman, F Claeyssens, N L Allan and J H Harding *Phys. Rev. Lett.* **96** 066102 (2006)
[15] H Şahin, S Cahangirov, M Topsakal, E Bekaroglu, E Akturk, R T Senger and S Ciraci *Phys. Rev. B—Condensed Matter Mater. Phys.* **80** 155453 (2009)
[16] M-Q Le *J. Comput. Theor. Nanosci.* **11** 1458 (2014)
[17] H Lu, Y Guo and J Robertson. *J. Appl. Phys.* **120** (2016)
[18] M S Prete, A Mosca Conte, P Gori, F Bechstedt and O Pulci. *Appl. Phys. Lett.* **110** (2017)
[19] A Friedrich, B Winkler, K Refson and V Milman *Phys. Rev. B—Condensed Matter Mater. Phys.* **82** 224106 (2010)
[20] E Deligoz, K Colakoglu, H B Ozisik and Y O Ciftci *Solid State Commun.* **151** 1122 (2011)
[21] R Zhang, Z Lin, H-K Mao and Y Zhao *Phys. Rev. B—Condensed Matter Mater. Phys.* **83** 060101 (2011)
[22] V V Bannikov, I R Shein and A L Ivanovskii *Phys. Status Solidi B* **248** 1369 (2011)
[23] X Hao, Y Xu, Z Li, L Wang, F Gao and D Xiao *Phys. Status Solidi B* **248** 2107 (2011)
[24] N Miao, B Sa, J Zhou, Z Sun and R Ahuja *Solid State Commun.* **151** 1842 (2011)
[25] Y Liang, X Yuan and W Zhang *J. Appl. Phys.* **109** (2011)
[26] R Yu, Y Jiang and R Zhou *Solid State Commun.* **186** 32 (2014)
[27] P Ordejón, E Artacho and J M Soler *Phys. Rev. B* **53** R10441 (1996)
[28] J P Perdew, K Burke and M Ernzerhof *Phys. Rev. Lett.* **77** 3865 (1996)
[29] N Troullier and J L Martins *Phys. Rev. B* **43** 1993 (1991)
[30] H J Monkhorst and J D Pack *Phys. Rev. B* **13** 5188 (1976)
[31] R Hundt, J C SchoÈn, A Hannemann and M Jansen *J. Appl. Crystallogr.* **32** 413 (1999)
[32] A Hannemann, R Hundt, J Schön and M Jansen *J. Appl. Crystallogr.* **31** 922 (1998)
[33] X P Du, V C Lo and Y X Wang *J. Comput. Chem.* **33** 18 (2012)
[34] Z L Zhao, K Bao, D F Duan, X L Jin, F B Tian, D Li, B B Liu and T Cui *J. Superhard Mater.* **36** 288 (2014)
[35] A Friedrich, B Winkler, L Bayarjargal, W Morgenroth, E A Juarez-Arellano, V Milman, K Refson, M Kunz and K Chen *Phys. Rev. Lett.* **105** 085504 (2010)
[36] Q L Xia, L X Pan, Y D Peng, L Y Li, H Z Wang, R Bao and J H Yi *Key Eng. Mater.* **512** 883 (2012)
[37] F Mouhat and F-X Coudert *Phys. Rev. B* **90** 224104 (2014)
[38] P F Weck, E Kim and K R Czerwinski *Dalton Trans.* **40** 6738 (2011)
[39] V V Bannikov, I R Shein and A L Ivanovskii *Phys. B Condens. Matter* **405** 4615 (2010)
[40] M A Ali, M M Hossain, M M Uddin, A Islam, D Jana and S H Naqib *J. Alloys Compd.* **860** 158408 (2021)
[41] J Worgull, E Petti and J Trivisonno *Phys. Rev. B* **54** 15695 (1996)
[42] M M Hossain and S H Naqib *Mol. Phys.* **118** e1609706 (2020)
[43] W Feng and S Cui *Can. J. Phys.* **92** 1652 (2014)
[44] D G Pettifor *Mater. Sci. Technol.* **8** 345 (1992)
[45] L Kleinman *Phys. Rev.* **128** 2614 (1962)
[46] A Makishima and J D Mackenzie *J. Non-Cryst. Solids* **17** 147 (1975)
[47] J J Wortman and R A Evans *J. Appl. Phys.* **36** 153 (1965)
[48] M I Naher, M A Afzal and S H Naqib *Results Phys.* **28** 104612 (2021)
[49] R Hill *First-principles elastic constants for the hcp transition metals Fe, Co, and Re at high pressure* p 350 (1952)
[50] W Voigt *Ann Arbor Mich BG Teubner JW Edw.* (1946)
[51] A Reuss *Z. Angew. Math. Mech.* **9** 49 (1929)
[52] S F Pugh *Lond. Edinb. Dublin Philos. Mag. J. Sci.* **45** 823 (1954)
[53] M Mahamudujjaman, M A Afzal, R S Islam and S H Naqib *AIP Adv.* **12** 025011 (2022)
[54] O L Anderson and H H Demarest Jr *J. Geophys. Res.* **76** 1349 (1971)
[55] G N Greaves, A L Greer, R S Lakes and T Rouxel *Nat. Mater.* **10** 823 (2011)
[56] L Vitos, P A Korzhavyi and B Johansson *Nat. Mater.* **2** 25 (2003)
[57] M J Phasha, P E Ngoepe, H R Chauke, D G Pettifor and D Nguyen-Mann *Intermetallics* **18** 2083 (2010)
[58] Z Sun, D Music, R Ahuja and J M Schneider *Phys. Rev. B* **71** 193402 (2005)
[59] S-H Jhi, J Ihm, S G Louie and M L Cohen *Nature* **399** 132 (1999)
[60] D M Teter *MRS Bull.* **23** 22 (1998)
[61] Y Tian, B Xu and Z Zhao *Int. J. Refract. Met. Hard Mater.* **33** 93 (2012)
[62] N Miao, B Sa, J Zhou and Z Sun *Comput. Mater. Sci.* **50** 1559 (2011)

[63] E Mazhnik and A R Oganov *J. Appl. Phys.* **126** 125109 (2019)
[64] X-Q Chen, H Niu, D Li and Y Li *Intermetallics* **19** 1275 (2011)
[65] M I Naher and S H Naqib *Results Phys.* **37** 105507 (2022)
[66] P Yang, H Fu, X Guo, B Rachid and J Lin *J. Mater. Res. Technol.* **9** 3109 (2020)
[67] P Ravindran, L Fast, P A Korzhavyi, B Johansson, J Wills and O Eriksson *J. Appl. Phys.* **84** 4891 (1998)
[68] X Gao, Y Jiang, R Zhou and J Feng *J. Alloys Compd.* **587** 819 (2014)
[69] C M Kube *AIP Adv.* **6** 095209 (2016)
[70] S I Ranganathan and M Ostoja-Starzewski *Phys. Rev. Lett.* **101** 055504 (2008)
[71] Ç Yamçıçıer *Indian J. Phys.* (2022)
[72] F Vahldiek *Anisotropy in Single-Crystal Refractory Compounds* (Springer) (2013)
[73] D H Chung and W R Buessem *J. Appl. Phys.* **38** 2010 (1967)
[74] Ç Yamçıçıer *Int. J. Hydrog. Energy* (2023)
[75] M I Naher and S H Naqib *Sci. Rep.* **11** 5592 (2021)
[76] J Wang, Y Zhou, T Liao and Z Lin *Appl. Phys. Lett.* **89** 021917 (2006)
[77] Z Ran, C Zou, Z Wei and H Wang *Comput. Phys. Commun.* **283** 108540 (2023)
[78] F Parvin and S H Naqib *Results Phys.* **21** 103848 (2021)
[79] J-H Xu, T Oguchi and A J Freeman *Phys. Rev. B* **35** 6940 (1987)
[80] E N Koukaras, G Kalosakas, C Galiotis and K Papagelis *Sci. Rep.* **5** 12923 (2015)
[81] Y Yun, D Legut and P M Oppeneer *J. Nucl. Mater.* **426** 109 (2012)
[82] G Kresse, J Furthmüller and J Hafner *EPL Europhys. Lett.* **32** 729 (1995)
[83] O L Anderson *J. Phys. Chem. Solids* **24** 909 (1963)
[84] E Schreiber, O L Anderson, N Soga and J F Bell (1975)
[85] M I Naher, M Mahamudujjaman, A Tasnim, R S Islam and S H Naqib *Solid State Sci.* **131** 106947 (2022)
[86] L D Brown, M E Fine and H L Marcus *Scr. Metall.* **18** 951 (1984)
[87] D S Clarke *Communicative Intent and Conventionality*, (Springer) p 67 (2003)
[88] G A Slack *Solid State Phys.* **34** 1 (1979)
[89] M Dressel and G Grüner (2002)
[90] S Li, R Ahuja, M W Barsoum, P Jena and B Johansson *Appl. Phys. Lett.* **92** (2008)